

Title: Comprehensive studies on sulfonated octaphenyl polyhedral silsesquioxane (SPOSS) using sulfuric acid: Structural analysis and composite crosslinked SPPSU/SPOSS membranes

Authors:

Fatin Bazilah Fauzi^a

Email: fatinbazilah89@gmail.com

Je-Deok Kim^{a,b}

Email: kim.jedeok@nims.go.jp

Affiliations:

^aFunctional Clay Materials Group, Functional Materials Research Center, National Institute for Materials Science, 1-1 Namiki, Tsukuba 305-0044, Japan

^bEnvironmental Circulation Composite Materials Group, Functional Materials Field, Research Center for Electronics and Optical Materials, National Institute for Materials Science, 1-1 Namiki, Tsukuba 305-0044, Japan

Corresponding author:

Je-Deok Kim – *Environmental Circulation Composite Materials Group, Functional Materials Field, Research Center for Electronics and Optical Materials, National Institute for Materials Science, 1-1 Namiki, Tsukuba 305-0044, Japan; orcid.org/ 0000-0003-4301-1044; Email: kim.jedeok@nims.go.jp*

Comprehensive studies on sulfonated octaphenyl polyhedral silsesquioxane (SPOSS) using sulfuric acid: Structural analysis and composite crosslinked SPPSU/SPOSS membranes

Fatin Bazilah Fauzi,^a Je-Deok Kim,^{a,b*}

^a Functional Clay Materials Group, Functional Materials Research Center, National Institute for Materials Science, 1-1 Namiki, Tsukuba 305-0044, Japan

^b Environmental Circulation Composite Materials Group, Functional Materials Field, Research Center for Electronics and Optical Materials, 1-1 Namiki, Tsukuba 305-0044, Japan

Abstract

We prepared sulfonated octaphenyl polyhedral silsesquioxane (SPOSS) with its structure intact by using sulfuric acid (H_2SO_4) at 40 °C. We discussed the effects of sulfonation using either chlorosulfonic acid (ClSO_3H) and H_2SO_4 on SPOSS structure and its incorporation into crosslinked sulfonated polyphenylsulfone (CSPPSU) composite polymer electrolyte membranes (PEM). An in-depth structural characterization using ^{29}Si NMR and FTIR spectroscopies, MALDI-TOF mass spectrometry, and TGA show that phenyl loss occurred in SPOSS prepared using ClSO_3H , resulting in a low ion exchange capacity (IEC) of 1.7 meq/g and a sulfonation degree (DS) of 1.9. In contrast, the phenyl remained intact in the SPOSS prepared using H_2SO_4 . Well-dispersed 348-nm-SPOSS- H_2SO_4 was found to have an IEC of 2.4 meq/g and DS of 3.1. The resultant hybrid PEM of CSPPSU/SPOSS using SPOSS- H_2SO_4 had improved swelling, mechanical and chemical strength, and conductivity. 1 wt% of SPOSS- H_2SO_4 loading had the highest conductivity (13.7 mS/cm) at 120 °C with 40% RH. This shows the importance of the SPOSS nanocomposite structure in dispersions in the SPPSU polymer matrix and its performance as PEM. We report on an improved direct sulfonation process at a milder condition but sulfonation yield was improved.

Keywords: Polymer electrolyte membrane; sulfonated octaphenyl polyhedral oligomeric silsesquioxane; nanocomposite; crosslinked SPPSU/SPOSS membrane.

1. Introduction

Greenhouse gas emission is a significant environmental problem, and 16% of worldwide CO₂ was produced from the transport sector in 2016 [1]. Green vehicles like plug-in hybrid and electric cars are already marketed as highly efficient and zero-emission alternatives. However, due to low battery performance, most are still limited to light-duty vehicles. A battery must be repeatedly recharged, resulting in decreased battery life and frequent replacement [2]. Compared to batteries, polymer electrolyte membrane fuel cells (PEMFC) have a higher energy density and faster charging rate. Recent PEMFCs have shown improvements and have started to exceed the batteries currently used [3]. PEMFCs are simple, light, and small, making them suitable for heavy-duty, long-range, high-utilization transportation means, such as buses, trucks, and trains [4,5].

Currently, commercially available polymer electrolyte membranes (PEMs) comprise poly(perfluorosulfonic acid) (PFSA), like Nafion, which has a well-connected ion path resulting in high conductivity in humid conditions [6,7]. In addition, it has high chemical resistance and mechanical strength due to the strong C–F bonds. However, the biggest challenges for PFSA are its poor performance at high temperatures (>80 °C) and low relative humidity (20% RH) [8-11]. Nafion conductivity was 6.6 mS/cm under those conditions [12]. Moreover, PFSA has a high production cost, and the waste is potentially hazardous [11,13,14]. To overcome the drawbacks of PFSA, the use of a sulfonated aromatic hydrocarbon-based polymer as a greener and more economical PEM material has attracted tremendous interest.

Results using sulfonated aromatic hydrocarbons such as polyimide [15-17], polyetheretherketone [18-21], poly(arylene ether sulfone) [21,22], polyethersulfone [23,24] and polysulfone [25,26], have shown that these materials have good potential as alternatives to Nafion. The molecular chain containing an aromatic structure offers thermal and mechanical stability up to 200 °C, which is promising for high-temperature applications [27,28]. The polyphenylsulfone (PPSU) backbone includes electron-rich sites favorable for sulfonation, resulting in more sulfo groups per polymer [29]. Thus, sulfonated PPSU (SPPSU) based membranes have high ion exchange capacities (IECs). For instance, SPPSU prepared from the monomers bis(4-fluorophenyl)sulfone and 4,4'-biphenol have high conductivities in the range of 100–200 mS/cm, which are higher than that for Nafion. However, the sulfonation process is complicated, and the membrane's durability remains an issue due to extreme swelling and poor strength [30].

Kim et al. have comprehensively reported on developments in the large-scale fabrication of crosslinked SPPSU (CSPPSU) membranes for many applications [30-34]. The effects of the co-solvent and annealing and activation processes on the SPPSU membranes are discussed, and they have been shown to affect the conductivity. A large-area (280 cm²) CSPPSU membrane activated to remove the by-products has been reported to have a swelling of 43% and a high tensile modulus of 48 MPa. The fuel cell using this CSPPSU has been shown to be stable up to 4000 h. However, the IEC was less than 2 meq/g, and the conductivity was 16 mS/cm (80 °C, 85% RH) [12].

Hybrid composite membranes can overcome low proton conductivities while enhancing the

membrane strength. Commonly used materials are inorganic composites with a high surface area and thermal and mechanical strengths [35-37]. These composite additives also improve membrane water retention and maintain ionic channels at high temperatures [38]. Hygroscopic oxides such as SiO₂, CeO₂, TiO₂, and ZrO₂ were reported to enhance the proton conductivity at low relative humidity conditions and the water retention of membranes [39]. However, the weak interaction between the polymer matrix and such composites makes homogeneous mixing difficult. In an effort to improve the weak interaction, recent reports on sulfonated carbon nanostructures as additives were shown to improve the strength and performance of aromatic hydrocarbon-based PEM [40-42]. Currently, controlling the size and aggregation of nanomaterials adequate to the ionic channel remains challenging [43].

Hydrophilic hybrid inorganic-organic particles, such as sulfonated octaphenyl polyhedral oligomeric silsesquioxane (SPOSS), show promising IECs due to the eight phenyl rings available for sulfonation. SPOSS has been commonly prepared using the superacid ClSO₃H. This method produces smaller particle sizes with a high degree of sulfonation, reaching 8 [44-46]. However, controlling the sulfonation process at room temperature or higher is challenging, resulting in low yields [38]. Proper control of the sulfonation conditions at a lower temperature is necessary. Membranes prepared via sulfonation with a mixture of chloroform and diluted ClSO₃H have been reported to have IECs less than 0.5 meq/g [38, 47-49]. There has not been a thorough discussion on the sulfonation effects on the OPOSS structure. Although several studies have highlighted the agglomeration issue involving SPOSS, further studies are needed.

Previously, we have reported the preparation of SPOSS with an IEC of 7.84 meq/g. CSPPSU composite membranes fabricated with 2 wt% of SPOSS have fuel cell performances comparable to Nafion 117 at 80 °C (complete hydration). The SPOSS was sulfonated using ClSO₃H at 50 °C for 1 day, followed by vacuum distillation at 110 °C before washing and drying. Although highly sulfonated SPOSS was prepared, the SPOSS nanoparticles in the SPPSU polymer matrix were agglomerated and unevenly distributed [50].

In this report, we directly sulfonated commercially available OPOSS and thoroughly discuss the structures of SPOSS prepared using H₂SO₄ (pK_a = -2.8) and ClSO₃H (pK_a = -6.5). By using H₂SO₄, the sulfonation was more controllable, and the SPOSS suffered less damage, as confirmed by using NMR and FTIR spectroscopies, TGA, and MALDI-TOF mass spectrometry. Nearly double the number of sulfonic moieties retained in SPOSS prepared using H₂SO₄ compared to ClSO₃H. In comparison with the CSPPSU membrane reported by Kim et al. [12], the conductivity of the CSPPSU/SPOSS-H₂SO₄ composite membrane increased by 2.7 times to 43 mS/cm at 80 °C and 85% RH and by 5.5 times at 120 °C and 40% RH to 13.7 mS/cm, which is comparable to Nafion212. When ClSO₃H was used to prepare the SPOSS, the tensile modulus of the CSPPSU/SPOSS decreased below 700 MPa up to 10 wt%. However, when H₂SO₄ was used, it exceeded 1000 MPa. In-depth comparisons of both sulfonation methods for preparing SPOSS and its loading in the CSPPSU/SPOSS composite membranes show the importance of the SPOSS structural integrity in composite CSPPSU membranes.

2. Experimental

2.1 Materials

Polyphenylsulfone (PPSU; Radel R-5000 NT; Solvay Specialty Polymers Japan K.K.; $M_w = 50,000$), octaphenyl polyhedral oligomeric silsesquioxane (OPOSS; $C_{48}H_{40}O_{12}Si_8$; Hybrid Plastic Inc.), Nafion[®] PFSA membrane of NR-212 (~50 μm) and NR-211 (~25 μm) from DuPont, USA, concentrated sulfuric acid (H_2SO_4 ; 98.8%; Nacalai Tesque, Inc; CAS: 7664-93-9), chlorosulfonic acid ($ClSO_3H$; 97.0%; Nacalai Tesque, Inc; CAS: 7790-94-5), dimethyl sulfoxide (DMSO; Sigma-Aldrich Co., Ltd.; CAS: 67-68-5), sodium hydroxide (NaOH; 97.0%; Nacalai Tesque, Inc, Japan; CAS: 1310-73-2), and sodium chloride (NaCl; 99.5%; Nacalai Tesque, Inc, Japan; CAS: 7647-14-5) were used without any further purification.

2.2 Synthesis of SPPSU and SPOSS

Commercial PPSU was sulfonated through an electrophilic aromatic substitution reaction using a concentrated H_2SO_4 at 40–60 °C for 24–48 h, as shown in Fig. 1. The details of the sulfonation are described in a previous study [32]. The molecular weights of the SPPSUs were determined to be 395,692 (40 °C; 24 h) and 215,604 (60 °C; 48 h) by using gel permeation chromatography (TOSOH HLC-8220 GPC; Shimadzu GPC 850D column) at 60 °C with *N,N*-dimethyl formamide (DMF) as the eluent.

The sulfonation of OPOSS was performed using either concentrated H_2SO_4 or $ClSO_3H$. First, 8 g of OPOSS was dried at 80 °C for 48 h and then mixed with 400 ml of H_2SO_4 or $ClSO_3H$ while stirring in a digital oil bath (SOR-243D; SANSYO Co, Ltd.) under the conditions listed in Table 1. The solution was cooled in an ice bath, producing a white precipitate, which later was collected using vacuum suction filtration. The crude white product was transferred to a dialysis tubing cellulose membrane (Spectra/Por 6; molecular weight cut-off, MWCO = 1 kD) and repeatedly washed with deionized water (PURELAB Option-R7, 15 M Ω cm at 25 °C) until the pH was 7. The solution was again filtered using filter paper (Advantec 5A) to remove the large impurities. The filtrate was heated on a hot plate to obtain a concentrated SPOSS/ H_2O solution.

2.3 Ion exchange capacity (IEC) and degree of sulfonation (DS) of SPPSU and SPOSS

The IECs of the SPPSU and SPOSS polymers were determined using a titration method. Solid SPOSS was prepared by drying the SPOSS/ H_2O solution on a hot plate. SPOSS and SPPSU (5 mg) were immersed in 20 ml of 2 M NaCl for 24 h. The resulting acidic solution was titrated with 0.01 M NaOH. This method maximized the dissociation of the sulfonic acid group and gave the most accurate measurement of the IEC value [51]. IEC (milliequivalent per gram, meq/g) was calculated using eq. 1 (C is the concentration; V is the volume; W is the weight):

$$IEC \text{ (meq/g)} = (C_{NaOH} \text{ (M)} \times V_{NaOH} \text{ (ml)}) / W_{dry} \text{ (g)} \quad (1)$$

The degree of sulfonation (DS) was calculated using eq. 2, where M_w is the molecular weight of the

repeating unit of the polymer (R.U. of SPPSU = 400.45, SPOSS = 1033.53) and the sulfonic acid unit (SO₃ = 80.06). The IEC and DS of the SPPSU are the average of two SPPSU samples prepared at 40 °C for 24 h, and at 60 °C for 48 h.

$$DS = \frac{IEC \times M_w(R.U.) \times 0.001}{1 - (IEC \times M_w(SO_3) \times 0.001)} \quad (2)$$

¹H nuclear magnetic resonance (NMR) of SPPSU was performed using a similar approach to our previous report [31]. In eq.3, DS was calculated based on the peak area analysis of ¹H NMR spectrum plotted in Fig. S1, where *A_{abc}* and *A_{de}* are the sums of the area of the proton peaks of a,b,c,d and e found at the chemical shift range of 7.0 to 8.5 ppm [52,53]. The DS obtained from ¹H NMR and titration methods were 2.1 and 1.9, respectively. The sulfonation details, IECs, and DSs of the SPPSU and SPOSS are listed in Table 1.

$$DS = \frac{12 - [4 \times (A_{abc}/A_{de})]}{2 + (A_{abc}/A_{de})} \quad (3)$$

Table 1 Conditions for the sulfonation process of the SPPSU and SPOSS by using H₂SO₄ and ClSO₃H along with their IEC and DS values.

| Polymer | Acid | Temp. (°C) | Time (h) | IEC (meq/g) | DS |
|---------|--------------------------------|------------|----------|-------------|-----|
| SPPSU | H ₂ SO ₄ | 40 – 60 | 24 – 48 | 3.3 | 1.9 |
| SPOSS | ClSO ₃ H | –10 | 24 | 1.7 | 1.9 |
| SPOSS | H ₂ SO ₄ | 40 | 48 | 2.4 | 3.1 |

2.4 Structural characterizations of SPOSS

Solid sampling matrix-assisted laser desorption/ionization mass spectroscopy (MALDI-MS; JMS-S3000 SpiralTOF™; JEOL, Ltd.), ²⁹Si NMR spectroscopy (Avance 400 MHz; Bruker), and Fourier-transform infrared spectroscopy (FTIR, Nicolet 6700 FT-IR Spectrometer; Thermo Fisher Scientific) were performed to identify the type of molecular species, the bonds, and the structures of SPOSS nanoparticles. The thermal stability was determined using thermogravimetric analysis (TGA) (DTG 60AH; Shimadzu) in flowing nitrogen and oxygen gas with a flow rate of 600 sccm. The temperature increased at a rate of 4 °C/min. The thicknesses of the dried and swollen membranes were measured using a Digimatic thickness gauge (547-401 ABSOLUTE; Mitutoyo, Japan). SPOSS prepared using H₂SO₄ was dispersed in water, and the particle size was measured using dynamic light scattering (DLS, Particle size Analyzer ELSZneo; Laser wavelength: 660 nm).

2.5 CSPPSU/SPOSS composite membrane preparation

First, solvent exchange was performed to prepare various concentrations of SPOSS/DMSO from SPOSS/H₂O. DMSO (5 g) was added into SPOSS/H₂O while stirring at 80–100 °C until the water was removed entirely. Separately, 0.3 g of SPPSU was dissolved in 3 g of DMSO. To this solution (10 wt% SPPSU/DMSO), SPOSS/DMSO was slowly added while rapidly stirring, and the mixture was stirred for a few days until a clear, well-dispersed cast solution (5 g) was obtained. The SPPSU/SPOSS/DMSO solution was cast in a 70 mm petri dish. The 4-step drying and crosslinking process was performed at

60, 120, 160, and 180 °C for 24 h each in an oven (DKN 302; Yamato Scientific Co., Ltd.). ~50 μm-thickness of CSPPSU/SPOSS composite membranes with SPOSS loading in the range of 1–50 wt% were prepared and then activated by immersion into 0.5 M NaOH, followed by 1 M H₂SO₄ for 24 h each, alternating with thoroughly washing in DI water. Activation is a crucial procedure to remove the by-products obstructing the ion-conducting path [12]. Lastly, the activated CSPPSU/SPOSS membranes were dried at RT for 24 h.

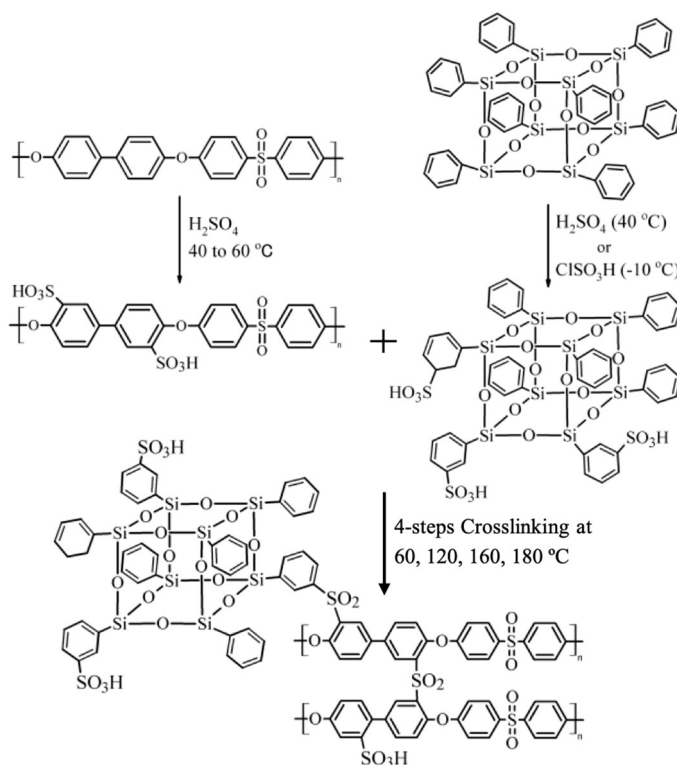


Fig. 1 Schematic representation of the structure of SPPSU, SPOSS and crosslinked SPPSU/SPOSS composite membrane.

2.6 CSPPSU/SPOSS composite membrane characterizations

TGA, X-ray fluorescence spectroscopy (XRF; ZSX PRIMUS II; Rigaku), and a Tension Test Machine (EZ-S, Shimadzu) were used to evaluate the thermal/mass properties, elemental analysis, and the stress-strain of the CSPPSU/SPOSS composite membranes. Microstructure studies were done using small angle X-ray scattering (SAXS) in the beamline of BL-6A (Wavelength: 0.15 nm; Camera length: 1000 mm; KEK Tsukuba, Japan). The average spacing calculated from Bragg's equation is ascribed to the average dimension of the ionic cluster using eq. 4. L is the average spacing (nm), and q is the scattering vector, which is expressed as eq. 5, with 2θ as the scattering angle and λ as the X-ray wavelength [12,54,55].

$$L = 2\pi/q \quad (4)$$

$$q = 4\pi/\lambda \sin\theta \quad (5)$$

3

2.7 Ion exchange capacity (IEC), degree of crosslinking (DCL), water uptake (WU), hydration number (λ), and oxidation stability of CSPPSU/SPOSS composite membrane

The IEC of the composite membrane before the crosslinking was estimated using eq. 6 (m is the mass fraction) [45]. The IEC after the crosslinking was determined using a titration method (eq. 1).

$$\text{IEC}_{\text{bef}} (\text{meq/g}) = (\text{IEC}_{\text{SPPSU}} \times m_{\text{SPPSU}}) + (\text{IEC}_{\text{SPOSS}} \times m_{\text{SPOSS}}) \quad (6)$$

Eq. 7 was used to calculate the composite membrane's DCL from the changes in the membrane's IEC before and after crosslinking.

$$\text{DCL} (\%) = ((\text{IEC}_{\text{bef}} - \text{IEC}_{\text{aft}})/\text{IEC}_{\text{bef}}) \times 100 \quad (7)$$

Water uptake (WU) was calculated from the weight difference between the dry and swollen state using eq. 8. The membrane was dried at 80 °C for 24 h to measure dry weight, and W_{dry} and W_{wet} were measured with the membranes in a swollen state after being immersed in water for 1 h at RT and 100 °C. Hydration number (λ) was then calculated using eq. 9:

$$\text{WU} (\%) = ((W_{\text{wet}} - W_{\text{dry}})/W_{\text{dry}}) \times 100 \quad (8)$$

$$\lambda([\text{H}_2\text{O}]/[\text{SO}_3\text{H}]) = 1000(W_{\text{wet}} - W_{\text{dry}})/(18 \times W_{\text{dry}} \times \text{IEC}) \quad (9)$$

A simple Fenton's test was done to evaluate the oxidative stability of the CSPPSU/SPOSS composite membranes following the previous report [12]. The interaction of aqueous H_2O_2 with the Fe^{2+} ion formed peroxy/hydroxyl radicals, which react with the polymer and initiate its chemical decomposition [13].

22

2.8 Proton conductivity of CSPPSU/SPOSS composite membrane

Proton conductivities were measured using 4-probe impedance spectroscopy (1 Hz–1 MHz; peak-to-peak voltage, $V_{\text{PP}} = 10$ mV; MTS, Scribner Associates, Inc.) in the temperature range of 40–120 °C with a series of relative humidities from 0% to 85%. The chamber was pressurized to 130 kPa for $T > 100$ °C measurements. The proton conductivities were calculated on the basis of the resistances obtained from the Nyquist plot (d is the thickness of the membrane (cm); A is the cross-sectional area of the membrane (cm^2); R is the resistance (Ω)).

$$\sigma (\text{S/cm}) = d/(A \times R) \quad (10)$$

The activation energy, (E_a , kJ/mol) was calculated from Arrhenius plots (eq. 11) for the proton conductivities at 40, 60 and 80 °C in the relative humidity range of 20%–80%. Here, σ is the proton conductivity, R is the gas constant (8.314 J/mol K), T is the temperature (K), and σ_0 is the pre-exponential factor (S/cm).

$$\ln \sigma = -\left(\frac{E_a}{R}\right)\left(\frac{1}{T}\right) + \ln \sigma_0 \quad (11)$$

36

2.9 Single cell performance of CSPPSU/SPOSS composite membrane

Large area membranes of 120 cm² was prepared by using a 10-cm-length knife applicator (Tester Sangyo CO., Ltd., Japan) using an automatic film-coating apparatus (KIPAE, KP-3000VH). Unlike small area membranes, casting solutions with higher concentration of 31 wt% in DMSO was used to fabricate membranes of CSPPSU and 1 wt% CSPPSU/SPOSS-H₂SO₄, casting at 60 °C (0.2-mm-gap; 20 mm/min speed). The membrane proceeded to a 5-step annealing treatment of 60 °C, 120 °C, 160 °C, and 180 °C for 90 minutes each step and at 200 °C for 12 hours. These crosslinked membranes were activated for 1 h at 80 °C in both 0.3 M of NaOH followed by 0.5 M of H₂SO₄. Membranes were washed until it became neutral in water after each step. After activation process, it was dried at RT for 24 h. Good, uniform, and transparent membranes with thicknesses of 30–40 μm were successfully prepared at a shorter annealing time and resisted high-temperature activation.

A single cell performance was performed on fuel cell system from AutoPEM of Toyo Corporation, Japan. The catalyst electrodes were 0.3 mg/cm² Pt/C/ionomer (ionomer/carbon=1) on GDL electrode. The membrane electrode assemblies (MEA) have an effective electrode area of 4 cm². The cell operated at atmospheric pressure, 80 °C temperature, and 100% RH. Feed gas supplied were 50 sccm pure H₂ and 100 sccm pure O₂ to the anode and cathode, respectively. Detailed information on the procedure can be found in our previous report [12].

3. Results and discussion

3.1 Structural characterization of SPOSS

Thermal decomposition of OPOSS and SPOSS in N₂ was observed using TGA, as shown in Fig. 2a. The first derivative weight loss curves indicate the temperatures of the maximum rate of change corresponding to the weight loss curves. In addition, TGA was performed under oxidative conditions using air, as shown in Fig. S2. The details of the weight loss percentage, the maximum degradation (T_{\max}), and the onset (T_{onset}) temperatures are listed in Table 2. The OPOSS had good thermal stability up to 350 °C, and its T_{onset} was 428 °C. Then, a two-step decomposition occurred with a total weight reduction of 29.3%. Decomposition of OPOSS under N₂ only allows sublimation and condensation to occur [49,50]. The T_{\max} was determined from the first derivative weight loss plot. The first T_{\max} was 428 °C, and the second was 595 °C. These steps represent the condensation of the phenyl groups and sublimation of the T8-caged POSS structure. Large char residues of about 70% yield at 600 °C are typical for POSS and depend strongly on decomposing the substituted grafted organic groups [56-58]. Longer aliphatic and aromatic substituents cause the polymerization of POSS, resulting in carbon entrapment and a larger amount of residue [59].

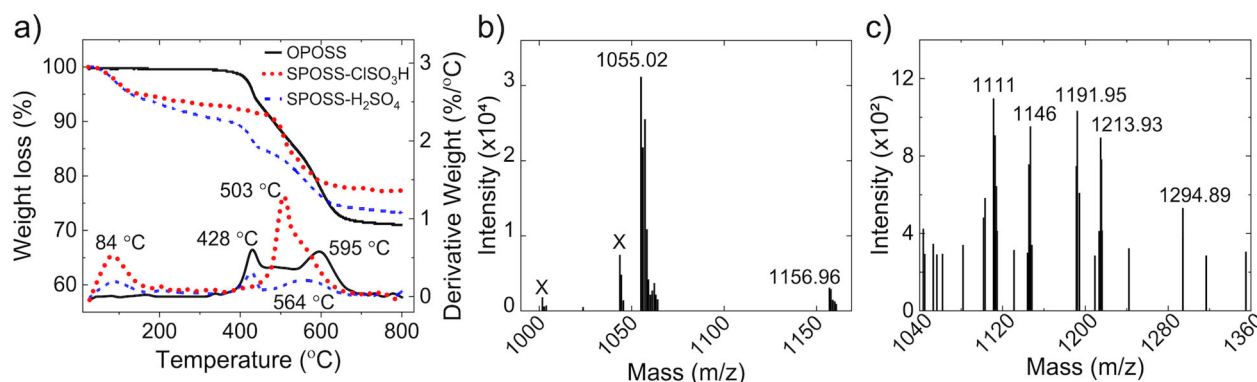


Fig. 2 a) TGA curves of SPOSS-H₂SO₄ and SPOSS-ClSO₃H with comparison to OPOSS in N₂ at 4 °C/min heating rate, MALDI-TOF mass spectrum of b) positive ions using DCTB (*trans*-2-[3-(4-*tert*-butylphenyl)-2-methyl-2-propenylidene]malononitrile) matrix and, c) negative ions using IAA (3-indoleacrylic acid) matrix of SPOSS-H₂SO₄ (Only peaks with intensity values above 300).

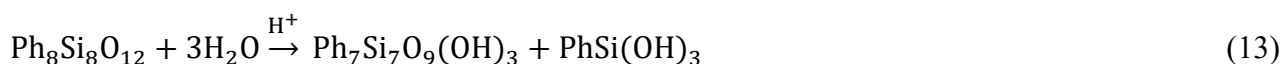
When SPOSS was prepared using H₂SO₄, a three-step decomposition was observed. The first weight loss of 5.6% was observed at 84 °C, and this was due to the evaporation of the bulk water associated with the sulfonic acid groups. Then, a weight loss of 3.2% occurred in the region of 150–350 °C due to the decomposition of sulfonic acid groups [13]. Weight losses of 19% were observed from the decomposition of the OPOSS backbone at T_{\max} values of 428 and 564 °C. The final residue was 72.2% of the original mass. The TGA curve for SPOSS-H₂SO₄ has a profile similar to that of the unsulfonated OPOSS. This indicates that the original OPOSS structure is maintained even after sulfonation. As shown later using MALDI-TOF, the OPOSS structure remained intact even after sulfonation using H₂SO₄ (Fig. 2b–2c).

In contrast, the TGA for SPOSS sulfonated by ClSO₃H only has a two-step weight loss. It starts with a weight loss of 5% at 84 °C from water attached to the sulfonic acid groups. The sulfonic acid gradually decomposed from 150–350 °C, resulting in a weight loss of 1.7%, almost half that of SPOSS-H₂SO₄. This reduced weight loss confirmed the lower degree of sulfonation and IEC values (Table 1). Only a one-step decomposition of the OPOSS backbone was observed at a T_{\max} of 503 °C with a weight loss of 16.2%, leaving a residue of 77%. The T_{onset} for SPOSS-H₂SO₄ was 125 °C, whereas it was 145 °C for the SPOSS-ClSO₃H. Attachment of the -SO₃H accelerates the decomposition of the polymer, leading to a lower T_{onset} [60]. This one-step decomposition differed significantly from those for OPOSS and SPOSS-H₂SO₄, strongly suggesting damage to the original silsesquioxane structure. A detailed analysis of its structure will be provided later.

Table 2 TGA data of the OPOSS and SPOSS prepared by H₂SO₄ and ClSO₃H.

| Sample | Weight loss (%) | | | T_{\max} (°C) | T_{onset} (°C) | Residue (%) |
|--------------------------------------|-----------------|------------|------------|-----------------|-------------------------|-------------|
| | RT–150 °C | 150–350 °C | 350–700 °C | | | |
| OPOSS | – | – | 29.3 | 428, 595 | 428 | 70.7 |
| SPOSS-H ₂ SO ₄ | 5.6 | 3.2 | 19.0 | 84, 428, 564 | 125 | 72.2 |
| SPOSS-ClSO ₃ H | 5.0 | 1.7 | 16.2 | 84, 503 | 145 | 77.1 |

The MALDI-TOF mass spectra of the SPOSS sulfonated using H₂SO₄ are shown in Fig. 2b and 2c. Please see the supporting information for the full range of the mass spectra (Fig. S3 and S4). In the positive ion mode in Fig. 2b, strong peaks appeared corresponding to the intact structure of OPOSS ($m/z = 1055$ for OPOSS-Na⁺) [61] and OPOSS-SO₃H ($m/z = 1157$ for OPOSS-SO₃Na-Na⁺). Sulfonation of the phenyl group increased the mass by 80. Simultaneously, side reactions resulting in broken cage structures of OPOSS are believed to have occurred in the presence of strong acids. Cage opening begins with bond cleavage of the Si-O bond through hydrolysis, as shown in eq. 12 [62]. This cleavage causes the molecular weight to increase by 17. In addition, further hydrolysis could result in the complete elimination of a Si-Ph vertex (eq. 13). In this case, the weight will be reduced by 108.



Thus, the phenyl loss and fragmentation of the Si-O-Si cage structure are expected to yield fragments with m/z values of 1174 (Ph₈Si₈O₁₁OH₂-Na⁺), 996 (Ph₇Si₈O₁₂OH-Na⁺), and 954 (Ph₇Si₇O₉OH₃-Na⁺) [63]. However, there are no such peaks apart from a weak peak at 955 m/z corresponding to the fragment shown in eq. 12 (Fig. S3). The broken structure was detected at $m/z = 955$, as shown in Fig. S5a.

The negative ion MALDI-TOF mass spectrum using an IAA (3-indoleacrylic acid) matrix was also acquired. The noise was much higher, and the intensity was lower in the negative ion mode due to measurement parameters and settings favoring higher signal intensities of the cations, disregarding the different mechanisms [64]. We re-plot the MALDI-TOF mass spectra to increase the intensity higher than 300 (Fig. 2c). Peaks for complete cages of OPOSS-SO₃⁻ ($m/z = 1111$) and OPOSS-(SO₃H)₂-H⁻ ($m/z = 1191.95$) were observed. Fragments believed to originate from the open cage structures were also detected. The fragments associated with the degree of sulfonation from one to three were observed at m/z values of 1146.31, 1213.93, and 1294.89, respectively (Fig. S5b–d)). The MALDI-TOF in the negative ion mode was used to confirm that sulfonation degrees of up to 3 ($m/z = 1294.89$ for Ph₈Si₈O₁₁OH₂-SO₃H₃-H⁻) were obtained. Both positive and negative mode MALDI-TOF mass spectra show that most of the phenyl groups remain intact in the structure of SPOSS-H₂SO₄.

Fig. 3a shows ²⁹Si NMR spectra of the SPOSS prepared using H₂SO₄ and ClSO₃H. The quaternary (Q_n) and trifunctional (T_n) structures were confirmed to be present in the SPOSS. Q_n is the notation for Si(Si-O)_n(OR)_{4-n} ($n = 1-4$), and T_n is the notation for PhSi(Si-O)_n(OR)_{3-n} ($n = 1-3$) [65]. For the original OPOSS, only a single T₃ peak for the PhSi(Si-O)₃ structure appeared at -78 ppm, corresponding to an eight vertex Ph-Si moiety. After sulfonation, hydrolysis of the Si-O-Si bond produced Q₂, Q₃, and Q₄ peaks at -91, -101, and -111 ppm, respectively. Concurrently, T₁ and T₂ peaks due to the dissociation of the phenyl groups, affording incomplete Ph-Si-O-Si bonds, were observed at -67 ppm and -77 ppm. The significant difference in the T₃ peak intensity indicates phenyl loss during sulfonation using ClSO₃H [38, 48]. A sharp T₃ peak for SPOSS-H₂SO₄ remained,

1 suggesting a higher proportion of phenyl-Si bonds.

2 The control of the sulfonation process is essential as the Si-C bonds of the aromatic structure are
3 very sensitive to the strong electrophile substitution process [48]. Aromatic ring cleavage or Si
4 replacement with electrophiles has been reported to occur when a mixture of ClSO₃H and chloroform
5 is used [38,48]. As a result, the acid capacities of these sulfonation agents' resulting acids are lower
6 than that for complete sulfonation with no phenyl loss. In this case, complete sulfonation was one
7 SO₃H per phenyl. However, only 30%–40% of the phenyl groups remain attached to the POSS siloxane
8 skeleton [48]. A schematic of the aromatic electrophilic substitution of the OPOSS is illustrated in Fig.
9 3a, along with the ²⁹Si NMR spectra. *Meta*-substitution generally occurs when the sulfonic acid
10 electrophile replaces the hydrogen atom [38,49]. However, high acid concentration and sulfonation
11 temperatures cause the phenyl to dissociate through *ipso*-substitution of the Si atoms, producing an
12 unfunctionalized phenyl group [48]. Thus, the loss of the phenyl group led to drops in the IEC and
13 degree of sulfonation. Sulfonation of OPOSS using H₂SO₄ mainly occurred on the *meta*-position of
14 the phenyl ring with the electrophile of sulfonic acid. The phenyl remained bonded with the Si–O–Si
15 moiety of POSS, as confirmed by the intensity of the T₃ peak in the spectrum.

16 FTIR spectra for OPOSS and SPOSS prepared using H₂SO₄ and ClSO₃H are compared in Fig. 3b.
17 In the IR spectrum of OPOSS, a strong Si–O–Si peak at 1091 cm^{−1} (stretching vibrations) and an Si-
18 phenyl peak in the range of 760–690 cm^{−1} (bending vibrations) were observed. Weak peaks for the Si-
19 phenyl moiety appeared in the range of 1425–1590 cm^{−1} (bending vibrations), and aromatic C=C/C–H
20 bonds appeared in the range of 3000–3100 cm^{−1} (stretching vibrations) [49,66]. After the sulfonation
21 process, the peaks for the Si–phenyl and Si–O–Si moieties were broader due to the introduction of the
22 –SO₃H group. The appearance of out-of-plane bending at 936 cm^{−1} indicates *meta*-substitution of the
23 aromatic ring [38,67]. The sharp peak at 3750 cm^{−1} for SPOSS was assigned to an isolated Si–OH
24 group on silica [66]. Some of the cage structures of the POSS have been damaged during the
25 sulfonation, producing incomplete Si–O–Si bonds, which is supported by the ²⁹Si NMR spectra. A
26 broad OH peak appeared around 3400 cm^{−1}, showing hydrogen bonding with the sulfonic group [38].
27 These agree with the higher IEC of the SPOSS-H₂SO₄.

28 Fig. 3c shows normalized FTIR spectra in the range of 900–1300 cm^{−1}, which were assigned to the
29 Si–O–Si moiety. A peak for an unsulfonated OPOSS was observed at 1091 cm^{−1}. The peak for the
30 SPOSS-ClSO₃H shifted from 1091 cm^{−1} to 1100 cm^{−1}, and that for SPOSS-H₂SO₄ shifted to 1033 cm^{−1}.
31 These were assigned to the symmetric and asymmetric vibrations of the –SO₃H groups [46,49].

32 From the low T₃ peak intensity for SPOSS-ClSO₃H in the ²⁹Si NMR spectra, phenyl rings were lost,
33 causing a low degree of sulfonation (1.9). The TGA plot showed slight weight loss from 150–350 °C
34 (i.e., SO₃H decomposition). A structure for SPOSS-ClSO₃H is shown in Fig. 3d, where several phenyl
35 groups are dissociated and replaced by the hydroxyl functional groups and only one or two sulfonated
36 phenyl groups. This structure is consistent with SPOSS-ClSO₃H being hydrophilic. In contrast,
37 SPOSS-H₂SO₄ retains most of its phenyl; about three phenyls have been sulfonated. The SPOSS-
38 H₂SO₄ is relatively hydrophobic. We will show later that the swelling of the CSPPSU composited

membrane using SPOSS-ClSO₃H is much larger than that of SPOSS-H₂SO₄.

We used MALDI-TOF mass spectrometry and NMR spectroscopy to show that the SPOSS structures upon sulfonation by either H₂SO₄ or ClSO₃H were different. Sulfonation using H₂SO₄ is a more controllable process at higher temperatures with minimal damage to the OPOSS structure than that using ClSO₃H. Although some of the cage structure became damaged, we minimized the phenyl loss from the siloxane bond and increased the sulfonation yield of SPOSS-H₂SO₄ (Fig. 3d).

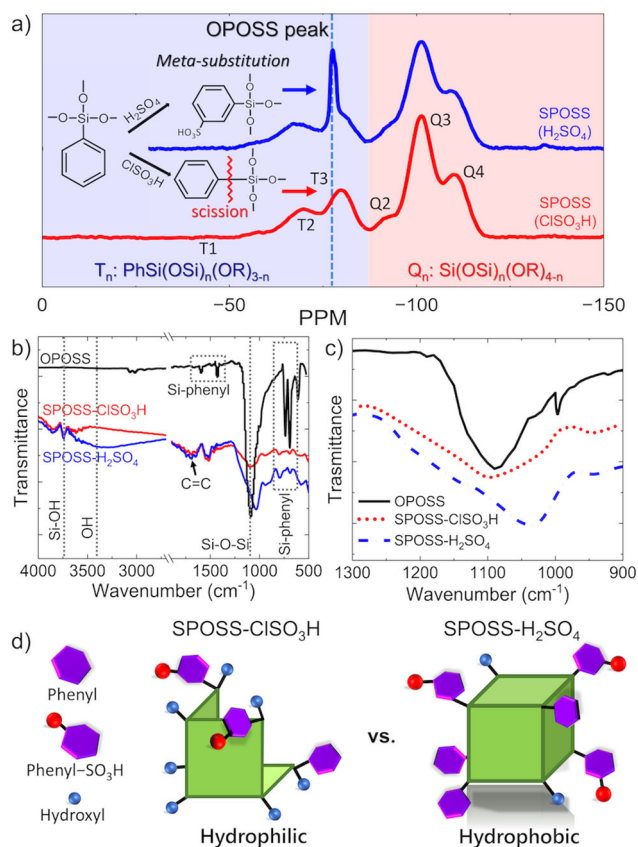


Fig. 3 a) ²⁹Si NMR spectra with structure assignment on the distinguishing peaks and the schematic diagram of the electrophilic substitution process using H₂SO₄ and ClSO₃H, (b) FTIR spectra of OPOSS (black), SPOSS-H₂SO₄ (blue) and -ClSO₃H (red), (c) Zoom in of normalized FTIR spectra at Si-O-Si peaks region, (d) Proposed structure of SPOSS-H₂SO₄ and SPOSS-ClSO₃H after the sulfonation.

3.2 IEC, DS, water uptake and stress-strain of crosslinked SPPSU/SPOSS membrane

SPOSS prepared from either H₂SO₄ or ClSO₃H were used to fabricate crosslinked SPPSU membranes and their IEC, DS, WU, and stress-strain characteristics were evaluated. Fig. 4a and 4b

1 compared their IECs before crosslinking (black dashed line) as estimated using eq. 6 to their IECs after
2 crosslinking (black solid line) as measured by titration. The degree of crosslinking was then calculated
3 from these values using eq. 7. After crosslinking, a maximum IEC of CSPPSU composite membrane
4 was obtained at 10 wt% and 5 wt% for SPOSS-H₂SO₄ and SPOSS-ClSO₃H, respectively. Degree of
5 crosslinking decreased to less than 5% as SPOSS concentration increased up to 50 wt%. The smaller
6 degree of crosslinking as SPOSS content increased suggests the formation of aggregates within the
7 composite polymers causes sulfonic acid groups unavailable as crosslinking sites [45]. Composite
8 CSPPSU membranes from SPOSS-ClSO₃H have a higher tendency to agglomerate more than from
9 SPOSS-H₂SO₄.

10 Fig. 4c shows the water uptake evaluation performed at room temperature and 100 °C for these
11 membranes. Composite membranes prepared using SPOSS-H₂SO₄ have low water uptake that does
12 not exceed 100% at room temperature and 300% at 100 °C for all concentration ranges. In contrast,
13 the addition of SPOSS-ClSO₃H into the membrane resulted in a large water uptake. At 50 wt% SPOSS-
14 ClSO₃H, water uptake was 2500% even at room temperature. Composite membranes prepared with 10
15 wt% or higher loading of SPOSS-ClSO₃H were found to disintegrate at 100 °C. The structure of
16 SPOSS prepared by ClSO₃H is much more hydrophilic and weaker than those prepared by H₂SO₄.

17 Fig. 4d and 4e show the tensile stress and strain of the CSPPSU/SPOSS composite membranes. The
18 average stress and strain strength of the CSPPSU membranes were determined to be 29 MPa and 118%,
19 respectively. The stress strength of CSPPSU/SPOSS-H₂SO₄ increased with an increase in the loading
20 and decreased when it was larger than 5 wt%. At 5 wt%, the stress strength increased by 21% to 35
21 MPa with a strain strength of 107%. In contrast, the mechanical strength of CSPPSU/SPOSS-ClSO₃H
22 decreased with an increase in the SPOSS-ClSO₃H loading. Adding 1 wt% SPOSS-ClSO₃H already
23 caused decreases in the tensile stress and strain by 31% and 15%, respectively. CSPPSU/SPOSS-
24 ClSO₃H is 10 MPa weaker than CSPPSU/SPOSS-H₂SO₄. The tensile modulus was calculated from
25 the stress-strain curve shown in Fig. 4f. The tensile modulus was improved by 40% when 1 wt% of
26 SPOSS-H₂SO₄ was incorporated into the CSPPSU polymer. In other words, the mechanical strength
27 of the CSPPSU composite membrane increases when SPOSS-H₂SO₄ is used, and it is stronger than
28 SPOSS-ClSO₃H.

29 CSPPSU/SPOSS-H₂SO₄ composite membrane has improved water swelling and high strength. The
30 improvements in mechanical strength also strongly suggest crosslinking between the SPPSU polymer
31 matrix and SPOSS additive. At 0% SPOSS, uncrosslinked SPPSU has a stress strength of 3 MPa,
32 which increases to 24 MPa after crosslinking. With the addition of 1% SPOSS, the crosslinked
33 membrane has a higher stress strength of 32 MPa. Identifying SO₂ crosslinks between SPPSU and
34 SPOSS remains challenging since the concentration of these crosslinks is too low to be directly
35 observed from FTIR or NMR [68]. The structure of SPOSS-H₂SO₄ was shown to be structurally intact
36 with the phenyl groups still available, and a much higher degree of sulfonation was achieved. We
37 believe that these factors are responsible for the significant improvements in the mechanical strength
38 of the composite membranes prepared with SPOSS-H₂SO₄ because the higher DS increased SPOSS

dispersibility within SPPSU polymer matrix, and more sulfonic acid group sites are available to crosslink to SPPSU. The membrane characteristics of the CSPPSU/SPOSS-ClSO₃H composite membranes are opposite, i.e., they are weaker due to extreme swelling and low strength. These results show the importance of the SPOSS structure as the nanocomposite in CSPPSU composite membranes. Phenyl loss and attachment of hydroxyl functional groups in the SPOSS-ClSO₃H disrupt the sulfonation process and weaken the CSPPSU/SPOSS composite membrane.

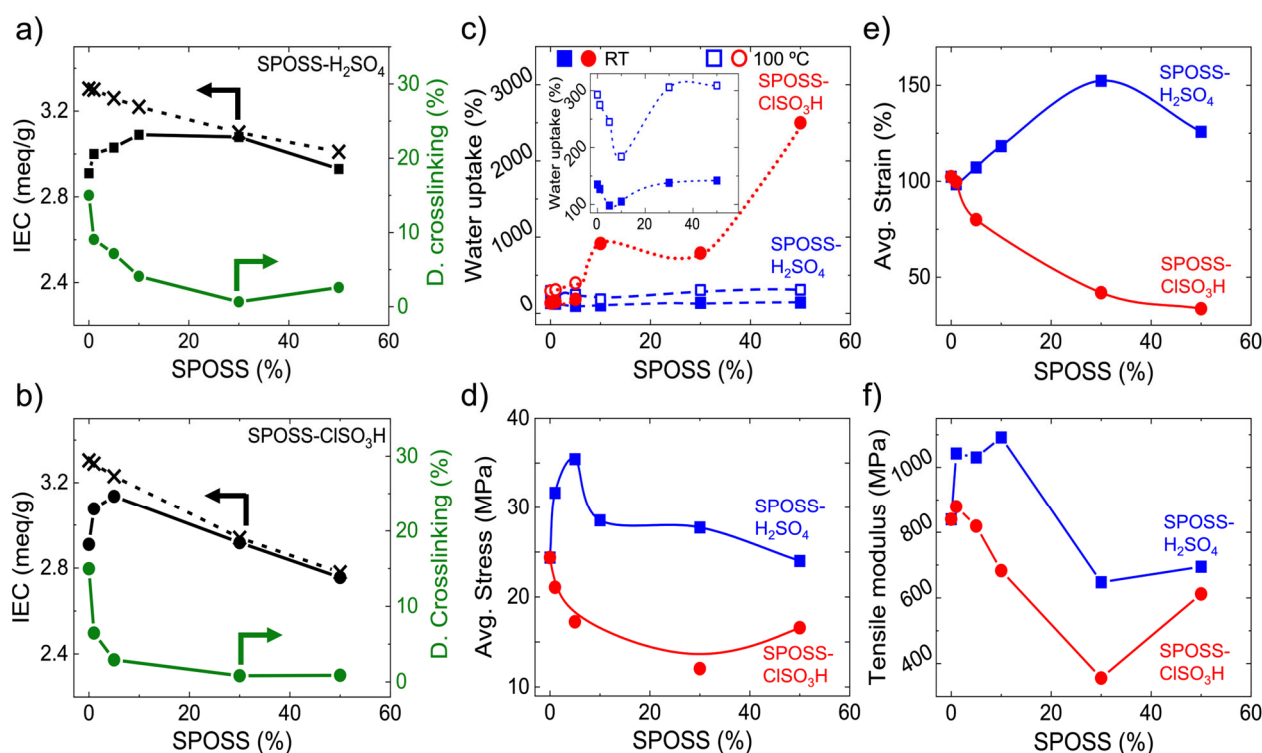


Fig. 4 IEC of the CSPPSU composite membrane using (a) SPOSS-H₂SO₄, (b) SPOSS-ClSO₃H (dashed line represents IEC before crosslinking (eq. 5)), (c) comparison of the WU of CSPPSU/SPOSS-H₂SO₄ and CSPPSU/SPOSS-ClSO₃H at RT and 100 °C (inset: enlargement of the WU plot for CSPPSU/SPOSS-H₂SO₄), and comparisons of (d) the average stress, (e) average strain and (f) tensile modulus of CSPPSU/SPOSS-H₂SO₄ and CSPPSU/SPOSS-ClSO₃H composite

3.3 Proton conductivity of crosslinked SPPSU/SPOSS membrane

Fig. 5a shows the proton conductivity of CSPPSU/SPOSS-H₂SO₄ at 80 °C against the SPOSS loading from 0 wt% to 50 wt%. CSPPSU membrane had a proton conductivity of 52.8 mS/cm at 85% RH. The conductivity of 1 wt% SPOSS-H₂SO₄ was found to be 46.7 mS/cm, and it gradually increased with the SPOSS loading. Only small changes of conductivity for all membranes were observed in the high humidity since the hydration numbers were all in the range of 50 – 60. Similar conductivities have been reported for measurements under full humidity conditions [46]. On the other hand, at higher temperature of 120 °C (Fig. 5b), the SPOSS loading significantly affected the conductivity. The CSPPSU membrane had a conductivity of 7.8 mS/cm at 40% RH. The 1 wt% of SPOSS-H₂SO₄

composite membrane had the highest proton conductivity of 13.7 mS/cm, a 75% improvement over that of CSPPSU. Incorporating 1 wt% SPOSS-H₂SO₄ improves the conductivity, making it comparable to Nafion212 (13.2 mS/cm). When the SPOSS loading was higher than 1 wt%, the conductivities decreased.

Fig. 5d and 5e show the conductivities of CSPPSU/SPOSS-ClSO₃H at 80 and 120 °C against the SPOSS loading from 0 wt% to 50 wt%. The conductivities increased with an increase in the SPOSS loading. At 50 wt% SPOSS-ClSO₃H loading, the highest conductivities of 58.49 mS/cm (85% RH) and 10.8 mS/cm (40% RH) at 80 and 120 °C, respectively, were obtained.

The activation energy (E_a), which is the minimum energy needed for the proton transfer from one free site to another. For the CSPPSU/SPOSS composite and Nafion 212 membranes were determined from temperature-dependent Arrhenius plots at 80% RH in the temperature range of 40–80 °C. The lower E_a , the better. The linear fitting ($R^2 > 0.91$) of the Arrhenius plot in Fig. 5c and 5f is equal to $-E_a/R$ (eq. 11). The CSPPSU membrane has a larger E_a (28.8 kJ/mol) than Nafion212 (19.3 kJ/mol), which is caused by the smaller ionic clusters. Incorporating 1 wt% SPOSS-H₂SO₄ into SPPSU reduced the E_a to 26.6 kJ/mol. Since similar E_a values were obtained at higher loading, a loading of 1 wt% is sufficient to improve proton transfer. The composite membrane with 1 wt% SPOSS-ClSO₃H had an E_a of 22.4 kJ/mol, and it increased with an increase in the SPOSS loading to 28.8 kJ/mol at 50 wt%. Although the CSPPSU/SPOSS-ClSO₃H composite membranes have lower E_a values, they are too weak to be used practically due to excessive water swelling and low mechanical strength.

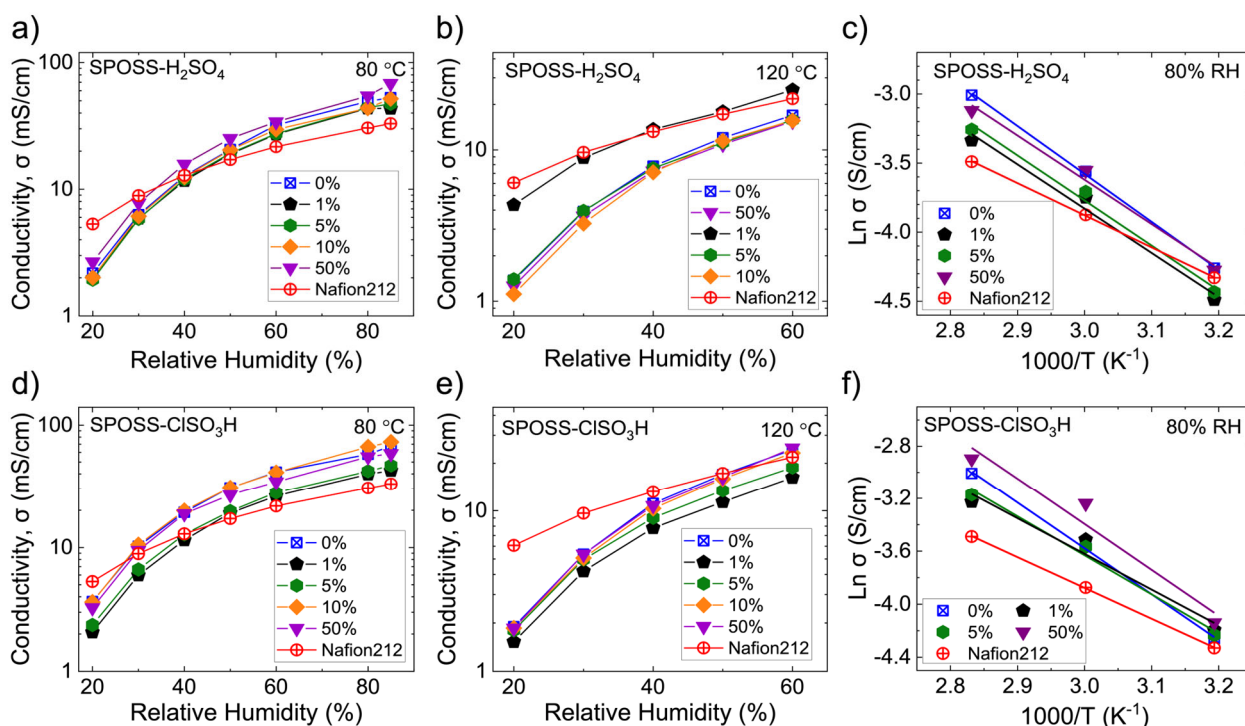


Fig. 5 (a–c) Proton conductivities at 80 and 120 °C and activation energy of CSPPSU/SPOSS-H₂SO₄, (d–f) Proton conductivities at 80 and 120 °C and activation energy of the CSPPSU/SPOSS-ClSO₃H in the T range of 40–80 °C at 80% RH.

At 120 °C, 1 wt% CSPPSU/SPOSS-H₂SO₄ was found to have the highest conductivity at 40% RH. A high SPOSS loading causes the aggregation of the SPOSS nanoparticles. A large aggregation of SPOSS initiates winding of and dead ends in the nano channels [69]. This causes the blocking of the hydrophilic domains and increases the tortuosity of the ionic path, resulting in a decrease in the conductivity [38,45-47]. Kugarajah et al. [47] have discussed that the aggregation pattern of the cluster network of POSS is similar to sulfonated POSS. Strong hydrogen bonds between Si-O-Si and SO₃H groups cause the aggregation of sulfonic moieties in SPOSS. However, in this study, there was no visible agglomeration observed on the membrane's surface, even at 50 wt% of SPOSS loading, as shown in Fig. S6a. SPOSS prepared using H₂SO₄ promotes the dispersion of the nanoparticles in the polymer matrix as the 30 wt% SPOSS in SPPSU/SPOSS cast solution was clear and transparent (Fig. S6b). Well-dispersed inorganic composites in the membrane are essential to enhance the synergistic effects of microscopic composite-type membranes on the thermal, mechanical, and chemical stabilities, which are not easy to achieve [35].

The visible agglomeration on the surface of the composite membranes at specific loadings of SPOSS has been reported when ClSO₃H was used to prepare the SPOSS [38,45,47,70]. The SPOSSs were not well dispersed and agglomerated with each other after the heat treatment process. In our previous study on the CSPPSU/SPOSS composite membrane, agglomeration occurred even at 2 wt% loading, as shown in Fig. S6c [50]. SPOSS was prepared using ClSO₃H at 50 °C. Although a high IEC of 7.86 was obtained, the dispersion of the SPOSS nanocomposite in the polymer matrix was poor.

3.4 Structural analysis and mechanical strength of crosslinked SPPSU/SPOSS membrane

The density of the sulfonic acids and the nanochannel for the ion mobility affect the conductivity of polymer membranes. Although higher IEC values are obtained with increased SPOSS loadings, poor mobility of the ion transfer inside the nanochannel can decrease the proton conductivity. The microstructure and reorganization of CSPPSU/SPOSS-H₂SO₄ composite membranes were analyzed

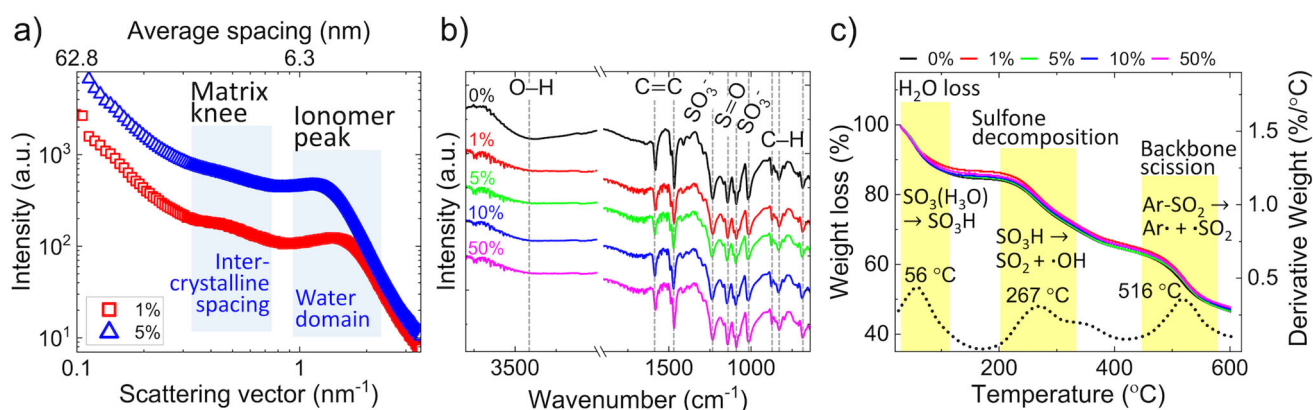


Fig. 6 (a) SAXS pattern of the membranes with SPOSS loadings of 1 wt% and 5 wt%, (b) FTIR spectra, and (c) TGA curves of 1 wt% to 50 wt% CSPPSU/SPOSS-H₂SO₄ composite membranes.

by using small-angle-X-ray-scattering (SAXS) with loadings of 1 wt% and 5 wt%, as shown in Fig. 6a. Two peaks appeared in the SAXS spectra of a swollen CSPPSU/SPOSS-H₂SO₄ membrane. The appearance of a shoulder peak between 0.3 nm⁻¹ and 0.8 nm⁻¹, known as the matrix knee, revealed the inter-crystalline spacing between the crystalline domains of the polymer matrix ($L = 20.9\text{--}7.9$ nm). The characteristic ionomer peak at $1\text{ nm}^{-1} < q < 2\text{ nm}^{-1}$ was attributed to a self-organized ionic cluster network under hydrated conditions. The scattering intensity of the ionomer peak is directly proportional to the difference in electron density of the polymer backbone and ionic clusters in SPOSS and SPPSU [13,54,55,71,72]. The ionic cluster size was calculated using the q value obtained from the plot made using eq. 4. Kim et al. [12] have reported that the CSPPSU membrane ionic cluster is 3.9 nm in size. Incorporating 1 wt% SPOSS-H₂SO₄ increased the size of the ionic cluster to 4.6 nm, and a loading of 5 wt% increased the cluster size to 5.5 nm. The addition of the SPOSS-H₂SO₄ increased the size of the ionic cluster, the IEC, and the hydration number of the CSPPSU/SPOSS-H₂SO₄ composite membranes. Although higher loadings increase the ionic cluster size, the proton conductivity at 120 °C decreased when SPOSS-H₂SO₄ loading > 1 wt%.

Kim et al. [45] have discussed the importance of controlling the aggregation in the nanochannel for good proton conductivity. From SAXS analysis, an SPOSS amount higher than 1.5 wt% in SPEEK composite membranes decreases the proton conductivity due to the aggregation of SPOSS in the nanochannel. An SPOSS loading of 5 wt% crowds and expands the nanochannel, which lowers the proton conductivity of the SPEEK/SPOSS composite membranes. Proton transfer in CSPPSU/SPOSS membranes with high water uptake occurs via a vehicular mechanism [8,73]. In our case, 1 wt% of SPOSS-H₂SO₄ is the optimal concentration in the CSPPSU/SPOSS membrane to improve the membrane strength and proton conductivity.

FTIR spectra of the CSPPSU and CSPPSU/SPOSS-H₂SO₄ membranes with different SPOSS loadings are shown in Fig. 6b. The presence of sulfonic acid groups was evidenced by the appearance of the peaks at 3400 (O–H vibrations), 1017, and 1238 cm⁻¹ (SO₃⁻ vibrations). The intensities of the O–H peaks were significantly reduced after adding the SPOSS-H₂SO₄ nanoparticles into the CSPPSU membrane. The addition of SPOSS-H₂SO₄ improved the membrane's water swelling and lowered SO₃H peaks due to the crosslinking among the moieties [50]. The C–H absorption peaks at 874, 829, and 686 cm⁻¹ were attributed to the C–H bond from the SPPSU polymer. Absorption peaks due to the C=C bonds in the benzene ring appeared at 1467 and 1581 cm⁻¹. The peaks at 1147 and 1088 cm⁻¹ were attributed to S=O bonds in the PPSU polymer backbone.

Fig. 6c shows the thermal decomposition of the CSPPSU/SPOSS-H₂SO₄ membranes by using TGA. Three weight loss stages were observed with thermolysis of distinct groups. The first step was the decomposition of water of H₃O⁺ associated with SO₃⁻ to SO₃H moieties at 56 °C. The second weight loss was the partial decomposition of SO₃H to SO₂ and ·OH at a maximum temperature of 267 °C, and the third weight loss was due to the decomposition of Ar-SO₂ in the PPSU backbone to Ar· and SO₂· at 516 °C [13,32,50,74]. The addition of SPOSS-H₂SO₄ increases the thermal stability of the CSPPSU

membranes from silicon in the POSS structures [47]. An SPOSS-H₂SO₄ loading of 1 wt% in CSPPSU increased the *T*_{90%} from 75 to 82 °C.

The Si content, which comes from the siloxane structure in the SPOSS, in the CSPPSU/SPOSS-H₂SO₄ composite membranes before and after activation was evaluated using X-ray fluorescence (XRF), as shown in Table 3. Before the activation, the Si content in the membranes was 10,000 ppm at an SPOSS-H₂SO₄ loading of 5 wt%. However, only 50 ppm of the Si remained in the membrane after activation. The same Si content was observed when the SPOSS loading was 10 wt%. When the SPOSS loading was 50 wt%, the Si content was only 100 ppm. This shows that the SiO₂ leaches during the NaOH activation process with SO₂ as a by-product. A large amount of the SPOSS nanocomposite is unnecessary since the amount of Si remains stagnant when SPOSS loading is higher than 5 wt%. In other words, material waste can be prevented since the SPOSS nanocomposite content does not affect the composite polymer much. This shows that only a small amount of the nanocomposite is incorporated into the polymer structure of the composite membranes. The amount of the

Table 3 XRF measurement of the amount of Si in the CSPPSU/SPOSS composite membranes before and after activation process.

| SPOSS (wt%) | Si content (ppm) |
|-------------------|------------------|
| 5 (No activation) | 10,000 |
| 5 | 50 |
| 10 | 50 |
| 50 | 100 |

nanocomposite should be in the order of parts per million (ppm). However, more studies on the range that might substantially improve the polymer membrane are needed.

Numerous studies have been reported on sulfonated POSS, which is used as a nanocomposite in hydrocarbon polymers. Table 4 compares the conductivity, swelling, and mechanical strength of the SPOSS composite polymer membranes in this study with previously reported membranes. In our research, we found that 1 wt% of the SPOSS composite was sufficient for the composite CSPPSU membranes. In comparison with our previous study, using sulfuric acid in the sulfonation process of the OPOSS is more controllable and causes less damage to the OPOSS structure. This significantly affects the distribution of the nanoparticles in the polymer matrix, and no visible agglomeration was observed on the membrane, even at a loading of 50 wt%. Agglomeration of SPOSS is a big problem since the nanoparticle distribution in the polymer plays a vital role in the membrane performance and strength. While conductivity results at 80 °C and >80% RH were shown to be much lower than other membranes in literature, not many studies measured conductivities at high-temperature and low-humidity conditions. At 120 °C and 40% RH, our CSPPSU/1 wt% SPOSS-H₂SO₄ has a very comparable conductivity of 13.7 mS/cm to Nafion212 (13.2 mS/cm) and other SPOSS composites aromatic hydrocarbon membranes. The oxidative stability of the CSPPSU membrane against Fenton's reagent improved from 2 to 4 h with the addition of SPOSS, suggesting future research on the CSPPSU composite membrane.

Table 4 IEC, conductivity, water uptake, stress-strain and oxidative stability data from the previous studies on the SPOSS composite membranes.

| | Sample | IEC (meg/g) | σ_1 (mS/cm) | σ_2 (mS/cm) | WU (%) RT, 100 °C | SS (MPa, %) | R _{oxidation} (%) | Ref. |
|------|--|----------------|-----------------------|-----------------------|----------------------|----------------|-------------------------------|------|
| | CSPPSU | 2.9 | 52.8 | 7.8 | 135, 293 | 29, 118 | 92 (2h) | a |
| | CSPPSU/ 1 wt%SPOSS | 3.0 | 46.7 | 13.7 | 120, 275 | 32, 98 | 100 (4h) | a |
| | CSPPSU/ 5 wt%SPOSS | 3.0 | 38.9 | 7.3 | 98, 245 | 35, 107 | 94 (4h) | a |
| | Nafion212 | 0.9 | 33.0 ^a | 13.2 ^a | 50, - | 16, >150 | 95 (48h) ⁷⁶ | 12 |
| 2023 | SPFEK/ 0.03 mg/cm ² SPOSS | - | 110 | - | 35.3, - | 47 | 95 (0.7h) | 77 |
| 2021 | Nafion/ 12 wt%SPOSS | - | 123 | - | 14, - | 25, 100 | 96 (36h) | 78 |
| 2020 | CSPPSU/ 1 wt%SPOSS | 1.9 | 37.9 | 6.6 | 128, - | 45, 66 | - | 50 |
| 2020 | CSPPSU/ 5 wt%SPOSS | 1.3 | 9.4 | 0.6 | 33, - | 52, 36 | - | 50 |
| 2020 | SPAES/ 2 wt%SPOSS | 2.1 | 163 | - | 48, 82 | 28, 8 | <100 (2h) | 75 |
| 2020 | SPEEK/ 5 wt% SPOSS | 1.8 | 13.1 ^b | - | 36, - | - | - | 47 |
| 2018 | SPEEK/ 1.5 wt%SPOSS | 1.5 | 97 | - | 31, - | 37, 70 | - | 45 |
| 2017 | PAES/ 14 wt%SPOSS | 1.4 | 142 | - | 21, 59 | 14, 45 | 95 (1h) | 79 |
| 2014 | Nafion/ 2 wt% SPOSS | 1.45 | 24 | - | 55, - | - | - | 67 |
| 2013 | SPEEK/ 2 wt%SPOSS | - | - | 0.036 ^c | 20.5, 80.3 | - | - | 70 |
| 2010 | CSPPSU/ 20 wt%SPOSS | 1.8 | 71 ^b | - | - | - | - | 46 |
| 2008 | CSPPSU/ 20 wt%SPOSS | - | 66 | - | 76 | 25, 4 | - | 44 |
| 2008 | CSPPSU/ 10 wt%SPOSS | - | 68 | - | 59 | 39, 9 | - | 44 |

σ^1 at 70–80 °C (85–100% RH); σ^2 at 120 °C (40% RH); WU is water uptake; SS is stress-strain; R_{oxidation} is oxidation stability;

^aOur data; ^bat room temperature; ^cat 100 °C

3.5 Single cell performance of crosslinked SPPSU/SPOSS membrane

The evaluation results for single cell performance of CSPPSU membranes with and without 1 wt% SPOSS were compared to the Nafion211 membrane. Each membranes have a thickness of 36, 31, and 25 μm . The electrochemical performances of the Pt/C/ionomer catalyst electrode were assessed by plotting the polarization curve and measuring the electrochemically active surface area (ECSA). Fig. 7a shows the I - V characteristic of a single cell at 80 °C and 100% RH, where $V_{\text{iR-free}}$ and $i_{\text{R-loss}}$ were plotted as the y-axes. Open circuit voltage (OCV) for all MEAs was in the range of 0.9 to 1.0 V, representing good assembly of PEM and the electrodes [75]. The current densities at 0.8 $V_{\text{iR-free}}$ were 66.6 mA/cm^2 , 118.3 mA/cm^2 , and 247.7 mA/cm^2 for CSPPSU/1wt%SPOSS- H_2SO_4 , CSPPSU, and

Nafion211, respectively. The voltage losses at 0.5 A/cm² were 143.6 mΩ, 102.2 mΩ, and 67.6 mΩ for CSPPSU/1wt% SPOSS-H₂SO₄, CSPPSU, and Nafion211, respectively. ECSA determined from CV measurement (Fig. 7b) were 65 m²/g, 68 m²/gPt, and 92 m²/gPt for CSPPSU/1wt%SPOSS-H₂SO₄, CSPPSU, and Nafion211, respectively. Although the conductivity of the CSPPSU and CSPPSU/1wt%SPOSS-H₂SO₄ membranes were higher than that of Nafion211 (Table 4), the fuel cell performance of the MEAs using CSPPSU and CSPPSU/1wt% SPOSS membranes was lower than that of Nafion211 due to the high iR loss (Fig. 7a). Furthermore, CV results show that the catalyst reaction at the anode and cathode electrodes of the MEA using CSPPSU/1wt% SPOSS membrane is lower than those of CSPPSU and Nafion211 membranes (Fig. 7b). The hydrogen crossover observed from the linear sweep voltammetry (LSV) are shown in Fig. 7c. Membranes of CSPPSU and CSPPSU/1wt%SPOSS-H₂SO₄ have a low current density of 0.3 mA/cm² at 0.4 V. However, Nafion211 has a higher current density at 1.8 mA/cm² at 0.4 V. CSPPSU, and CSPPSU/1wt%SPOSS-H₂SO₄ have a higher resistance to the hydrogen crossover in the fuel cell system. The results show a need for a high-performance fuel cell system using CSPPSU/1wt% SPOSS membrane to improve the interface resistance and catalyst reaction in the MEA.

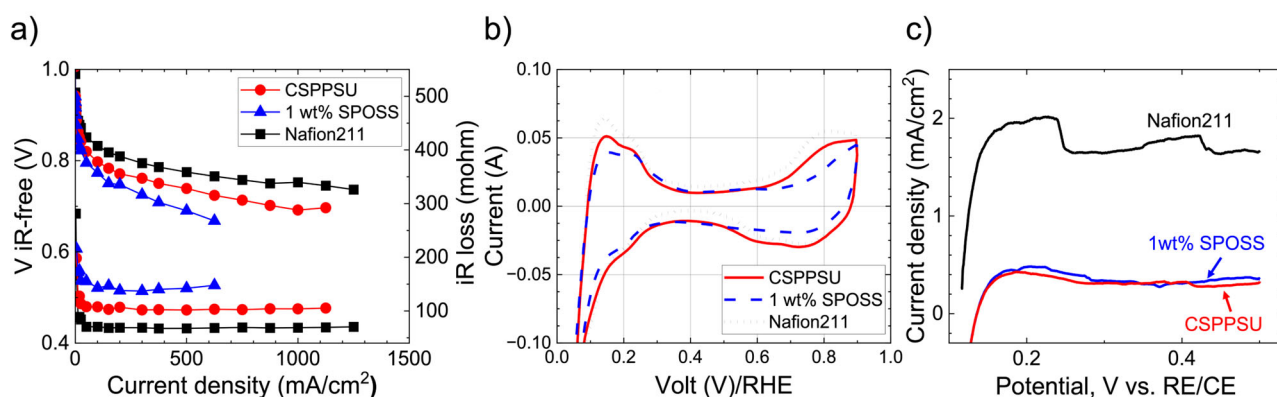


Fig. 7 (a) Polarization (b) cyclic voltammetry (CV), and (c) linear sweep voltammetry (LSV) of hydrogen crossover current curves of CSPPSU, CSPPSU/1 wt% SPOSS and Nafion211 at 80 °C, 100% RH.

4. Conclusions

In summary, direct sulfonation of OPOSS using H₂SO₄ was more controllable and could be performed under milder conditions to prevent damage to the SPOSS composite structure. Well-dispersed 348 nm-hydrophobic-SPOSS-H₂SO₄ with an IEC of 2.4 meq/g and DS of 3.1 was prepared. Structural analysis using ²⁹Si NMR and FTIR spectroscopies, MALDI-TOF mass spectrometry, and TGA confirmed that the phenyl remained intact in the T8-cage structure of OPOSS. In addition, incorporating 1 wt% SPOSS-H₂SO₄ into SPPSU improved the stability and strength of the crosslinked SPPSU/SPOSS composite membranes. The water uptake was reduced by 11%, and the tensile modulus was enhanced by 40% over the CSPPSU membrane. The proton conductivity at 120 °C and 40% RH was 13.7 mS/cm, which is similar to Nafion211 (13.2 mS/cm). From SAXS analysis, the ionic cluster

expanded proportionally with the SPOSS loading. However, SPOSS loadings higher than 1 wt% crowd the expanded ionic cluster, resulting in decreased conductivities. The improvements in the CSPPSU/SPOSS-H₂SO₄ composite membrane show the importance of the SPOSS structure as the nanocomposite. The sulfonation process using different acids is promising for producing good dispersions and intact SPOSS structure, which is a priority for PEM nanofillers.

CRedit authorship contribution statement

F.B. Fauzi: Methodology, Investigation, Formal analysis, Writing - Original Draft. **J.-D. Kim:** Conceptualization, Supervision, Funding acquisition, Methodology, Investigation, Formal analysis, Writing - Review & Editing.

Acknowledgement

This research was partly supported by the New Energy and Industrial Technology Development Organization (NEDO) through the “Collaborative Industry-Academia-Government R&D Project for Solving Common Challenges Toward Dramatically Expanded Use of Fuel Cells and Related Equipment”. Special thanks to Sachiko Takao for her assistance in the stress-strain measurements. Small-angle X-ray scattering (SAXS) measurements were performed at the Photon Factory (beamline BL6A) of KEK (proposal no. 2021G517). J.-D. Kim thanks Akihiro Ohira of the National Institute of Advanced Industrial Science and Technology (AIST) for their help with the SAXS measurements.

References

- [1] H. Ritchie, M. Roser, P. Rosado, CO₂ and Greenhouse Gas Emissions. <https://ourworldindata.org/co2-and-greenhouse-gas-emissions>, 2023 (accessed 1 July 2023).
- [2] R. Vinodh, R. Atchudan, H.-J. Kim, M. Yi, Recent Advancements in Polysulfone Based Membranes for Fuel Cell (PEMFCs, DMFCs and AMFCs) Applications: A Critical Review, *Polymers*. 14 (2022) 300.
- [3] Z.P. Cano, D. Banham, S. Ye, A. Hintennach, J. Lu, M. Fowler, Z. Chen, Batteries and fuel cells for emerging electric vehicle markets, *Nat. Energy*. 3 (2018) 279–289.
- [4] Y. Wang, K.S. Chen, J. Mishler, S.C. Cho, X.C. Adroher, A review of polymer electrolyte membrane fuel cells: Technology, applications, and needs on fundamental research, *Appl. Energy*. 88 (2011) 981–1007.
- [5] B.G. Pollet, S.S. Kocha, I. Staffell, Current status of automotive fuel cells for sustainable transport, *Curr. Opin. Electrochem*. 16 (2019) 90–95.
- [6] M.A. Hickner, H. Ghassemi, Y.S. Kim, B.R. Einsla, J.E. McGrath, Alternative Polymer Systems for Proton Exchange Membranes (PEMs), *Chem. Rev.* 104 (2004) 4587–4612.
- [7] Y. Wang, D.F. Ruiz Diaz, K.S. Chen, Z. Wang, X.C. Adroher, Materials, technological status, and fundamentals of PEM fuel cells – A review, *Mater. Today*. 32 (2020) 178–203.

- 1 [8] K. Firouz Tadavani, A. Abdolmaleki, M.R. Molavian, M. Zhiani, A Promising Proton-
2 Exchange Membrane: High Efficiency in Low Humidity, *ACS Appl. Energy Mater.* 1 (2018)
3 2464–2473.
- 4 [9] W. Jia, B. Tang, P. Wu, Novel Composite Proton Exchange Membrane with Connected Long-
5 Range Ionic Nanochannels Constructed via Exfoliated Nafion–Boron Nitride Nanocomposite,
6 *ACS Appl. Mater. Interfaces.* 9 (2017) 14791–14800.
- 7 [10] H. Nguyen, F. Lombeck, C. Schwarz, P.A. Heizmann, M. Adamski, H.-F. Lee, B. Britton, S.
8 Holdcroft, S. Vierrath, M. Breitwieser, Hydrocarbon-based PemionTM proton exchange
9 membrane fuel cells with state-of-the-art performance, *Sustain. Energy Fuels.* 5 (2021) 3687–
10 3699.
- 11 [11] X. Ge, F. Zhang, L. Wu, Z. Yang, T. Xu, Current Challenges and Perspectives of Polymer
12 Electrolyte Membranes, *Macromolecules.* 55 (2022) 3773–3787.
- 13 [12] J.-D. Kim, A. Ohira, H. Nakao, Chemically Crosslinked Sulfonated Polyphenylsulfone
14 (CSPPSU) Membranes for PEM Fuel Cells, *Membranes.* 10 (2020) 31.
- 15 [13] A. Kusoglu, A.Z. Weber, New Insights into Perfluorinated Sulfonic-Acid Ionomers, *Chem. Rev.*
16 117 (2017) 987–1104.
- 17 [14] M. Feng, R. Qu, Z. Wei, L. Wang, P. Sun, Z. Wang, Characterization of the thermolysis products
18 of Nafion membrane: A potential source of perfluorinated compounds in the environment, *Sci.*
19 *Rep.* 5 (2015) 9859.
- 20 [15] N. Asano, M. Aoki, S. Suzuki, K. Miyatake, H. Uchida, M. Watanabe, Aliphatic/Aromatic
21 Polyimide Ionomers as a Proton Conductive Membrane for Fuel Cell Applications, *J. Am.*
22 *Chem. Soc.* 128 (2006) 1762–1769.
- 23 [16] Q. Yuan, P. Liu, G.L. Baker, Sulfonated polyimide and PVDF based blend proton exchange
24 membranes for fuel cell applications, *J. Mater. Chem. A.* 3 (2015) 3847–3853.
- 25 [17] C.H. Lee, C.H. Park, Y.M. Lee, Sulfonated polyimide membranes grafted with sulfoalkylated
26 side chains for proton exchange membrane fuel cell (PEMFC) applications, *J. Memb. Sci.* 313
27 (2008) 199–206.
- 28 [18] R.P. Mariappan, C. Liu, G. Cao, R.P. Manimuthu, Tailoring SPEEK/SPVdF-co-HFP/La₂Zr₂O₇
29 Ternary Composite Membrane for Cation Exchange Membrane Fuel Cells, *Ind. Eng. Chem.*
30 *Res.* 59 (2020) 4881–4894.
- 31 [19] A.R. Kim, M.B. Poudel, J.Y. Chu, M. Vinothkannan, R. Santhosh Kumar, N. Logeshwaran, B.-
32 H. Park, M.-K. Han, D.J. Yoo, Advanced performance and ultra-high, long-term durability of
33 acid-base blended membranes over 900 hours containing sulfonated PEEK and quaternized
34 poly(arylene ether sulfone) in H₂/O₂ fuel cells, *Compos. Part B Eng.* 254 (2023) 110558.
- 35 [20] P. Xing, G.P. Robertson, M.D. Guiver, S.D. Mikhailenko, K. Wang, S. Kaliaguine, Synthesis
36 and characterization of sulfonated poly(ether ether ketone) for proton exchange membranes, *J.*
37 *Memb. Sci.* 229 (2004) 95–106.
- 38 [21] R. Hara, N. Endo, M. Higa, K. Okamoto, X. Zhang, H. Bi, S. Chen, Z. Hu, S. Chen, *Polymer*

electrolyte fuel cell performance of poly(arylene ether ketone)-graft-crosslinked-poly(sulfonated arylene ether sulfone), *J. Power Sources*. 247 (2014) 932–938.

[22] J. Kim, S. Hwang, Y.G. Jeong, Y.S. Choi, K. Kim, Cross-Linked Sulfonated Poly(arylene ether sulfone) Membrane Using Polymeric Cross-Linkers for Polymer Electrolyte Membrane Fuel Cell Applications, *Membranes*. 13 (2023) 7.

[23] M.L. Di Vona, G. Alberti, E. Sgreccia, M. Casciola, P. Knauth, High performance sulfonated aromatic ionomers by solvothermal macromolecular synthesis, *Int. J. Hydrogen Energy*. 37 (2012) 8672–8680.

[24] W. Mabrouk, L. Ogier, S. Vidal, C. Sollogoub, F. Matoussi, M. Dachraoui, J.F. Fauvarque, Synthesis and Characterization of Polymer Blends of Sulfonated Polyethersulfone and Sulfonated Polyethersulfone Octylsulfonamide for PEMFC Applications, *Fuel Cells*. 12 (2012) 179–187.

[25] C. Simari, M. Prejanò, E. Lufrano, E. Sicilia, I. Nicotera, Exploring the Structure–Performance Relationship of Sulfonated Polysulfone Proton Exchange Membrane by a Combined Computational and Experimental Approach, *Polymers*. 13 (2021) 959.

[26] C. Simari, E. Lufrano, A. Brunetti, G. Barbieri, I. Nicotera, Polysulfone and organo-modified graphene oxide for new hybrid proton exchange membranes: A green alternative for high-efficiency PEMFCs, *Electrochim. Acta*. 380 (2021) 138214.

[27] D.W. Shin, M.D. Guiver, Y.M. Lee, Hydrocarbon-Based Polymer Electrolyte Membranes: Importance of Morphology on Ion Transport and Membrane Stability, *Chem. Rev.* 117 (2017) 4759–4805.

[28] K. Jiao, J. Xuan, Q. Du, Z. Bao, B. Xie, B. Wang, Y. Zhao, L. Fan, H. Wang, Z. Hou, S. Huo, N.P. Brandon, Y. Yin, M.D. Guiver, Designing the next generation of proton-exchange membrane fuel cells, *Nature*. 595 (2021) 361–369.

[29] S. Swaby, N. Ureña, M. Teresa Pérez-Prior, C. del Río, A. Várez, J.-Y. Sanchez, C. Iojoiu, B. Levenfeld, Proton conducting sulfonated polysulfone and polyphenylsulfone multiblock copolymers with improved performances for fuel cell applications, *J. Ind. Eng. Chem.* 122 (2023) 366–377.

[30] Y. Zhang, J. Kim, K. Miyatake, Effect of thermal crosslinking on the properties of sulfonated poly(phenylene sulfone)s as proton conductive membranes, *J. Appl. Polym. Sci.* 133 (2016).

[31] J.-D. Kim, L.-J. Ghil, Annealing effect of highly sulfonated polyphenylsulfone polymer, *Int. J. Hydrogen Energy*. 41 (2016) 11794–11800.

[32] S. Matsushita, J.-D. Kim, Organic solvent-free preparation of electrolyte membranes with high proton conductivity using aromatic hydrocarbon polymers and small cross-linker molecules, *Solid State Ionics*. 316 (2018) 102–109.

[33] J. Kim, A. Donnadio, M. Jun, M.L. Di Vona, Crosslinked SPES-SPPSU membranes for high temperature PEMFCs, *Int. J. Hydrogen Energy*. 38 (2013) 1517–1523.

[34] J. Kim, A. Ohira, Crosslinked Sulfonated Polyphenylsulfone (CSPPSU) Membranes for

Elevated-Temperature PEM Water Electrolysis, Membranes. 11 (2021) 861.

- [35] C.H. Park, C.H. Lee, M.D. Guiver, Y.M. Lee, Sulfonated hydrocarbon membranes for medium-temperature and low-humidity proton exchange membrane fuel cells (PEMFCs), *Prog. Polym. Sci.* 36 (2011) 1443–1498.
- [36] C.Y. Wong, W.Y. Wong, K. Ramya, M. Khalid, K.S. Loh, W.R.W. Daud, K.L. Lim, R. Walvekar, A.A.H. Kadhum, Additives in proton exchange membranes for low- and high-temperature fuel cell applications: A review, *Int. J. Hydrogen Energy*. 44 (2019) 6116–6135.
- [37] T. Xu, Ion exchange membranes: State of their development and perspective, *J. Memb. Sci.* 263 (2005) 1–29.
- [38] S. Subianto, M.K. Mistry, N.R. Choudhury, N.K. Dutta, R. Knott, Composite Polymer Electrolyte Containing Ionic Liquid and Functionalized Polyhedral Oligomeric Silsesquioxanes for Anhydrous PEM Applications, *ACS Appl. Mater. Interfaces*. 1 (2009) 1173–1182.
- [39] H. Ranganathan, M. Vinothkannan, A.R. Kim, V. Subramanian, M. Oh, D.J. Yoo, Simultaneous improvement of power density and durability of sulfonated poly(ether ether ketone) membrane by embedding CeO₂-ATiO₂: A comprehensive study in low humidity proton exchange membrane fuel cells, *Int. J. Energy Res.* 46 (2022) 9041–9057.
- [40] M. Vinothkannan, A.R. Kim, S.K. Ryu, D.J. Yoo, Structurally modulated and functionalized carbon nanotubes as potential filler for Nafion matrix toward improved power output and durability in proton exchange membrane fuel cells operating at reduced relative humidity, *J. Memb. Sci.* 649 (2022) 120393.
- [41] X. He, G. He, A. Zhao, F. Wang, X. Mao, Y. Yin, L. Cao, B. Zhang, H. Wu, Z. Jiang, Facilitating Proton Transport in Nafion-Based Membranes at Low Humidity by Incorporating Multifunctional Graphene Oxide Nanosheets, *ACS Appl. Mater. Interfaces*. 9 (2017) 27676–27687.
- [42] A.R. Kim, M. Vinothkannan, S. Ramakrishnan, B.-H. Park, M.-K. Han, D.J. Yoo, Enhanced electrochemical performance and long-term durability of composite membranes through a binary interface with sulfonated unzipped graphite nanofibers for polymer electrolyte fuel cells operating under low relative humidity, *Appl. Surf. Sci.* 593 (2022) 153407.
- [43] L. Liu, Y. Lu, Y. Pu, N. Li, Z. Hu, S. Chen, Highly sulfonated carbon nano-onions as an excellent nanofiller for the fabrication of composite proton exchange membranes with enhanced water retention and durability, *J. Memb. Sci.* 640 (2021) 119823.
- [44] C. Hartmann-Thompson, A. Merrington, P.I. Carver, D.L. Keeley, J.L. Rousseau, D. Hucul, K.J. Bruza, L.S. Thomas, S.E. Keinath, R.M. Nowak, D.M. Katona, P.R. Santurri, Proton-conducting polyhedral oligosilsesquioxane nanoadditives for sulfonated polyphenylsulfone hydrogen fuel cell proton exchange membranes, *J. Appl. Polym. Sci.* 110 (2008) 958–974.
- [45] S.-W. Kim, S.-Y. Choi, H.-W. Rhee, A novel sPEEK nanocomposite membrane with well-controlled sPOSS aggregation in tunable nanochannels for fast proton conduction, *Nanoscale*. 10 (2018) 18217–18227.

- [46] B. Decker, C. Hartmann-Thompson, P.I. Carver, S.E. Keinath, P.R. Santurri, Multilayer Sulfonated Polyhedral Oligosilsesquioxane (S-POSS)-Sulfonated Polyphenylsulfone (S-PPSU) Composite Proton Exchange Membranes, *Chem. Mater.* 22 (2010) 942–948.
- [47] V. Kugarajah, S. Dharmalingam, Sulphonated polyhedral oligomeric silsesquioxane/sulphonated poly ether ether ketone nanocomposite membranes for microbial fuel cell: Insights to the miniatures involved, *Chemosphere.* 260 (2020) 127593.
- [48] E. Carlier, A. Revillon, A. Guyot, P. Baumgartner, Functional silica supported polymers IV. Synthesis and catalytic activity of silica-grafted sulfonated polyphenylsilsesquioxane, *React. Polym.* 21 (1993) 15–25.
- [49] V. Söderholm, J. Esteban, D. Vogt, Synthesis of a H-Sulfo-POSS catalyst and application in the acetalization of glycerol with 2-butanone to yield a biofuel additive, *Catal. Sci. Technol.* 11 (2021) 4529–4538.
- [50] N.A.M. Nor, J. Jaafar, J.-D. Kim, Improved properties of sulfonated octaphenyl polyhedral silsesquioxane cross-link with highly sulfonated polyphenylsulfone as proton exchange membrane, *J. Solid State Electrochem.* 24 (2020) 1185–1195.
- [51] N. Gospodinova, E. Tomšík, O. Omelchenko, How strong are strong poly(sulfonic acids)? An example of the poly(2-acrylamido-2-methyl-1-propanesulfonic acid), *Eur. Polym. J.* 74 (2016) 130–135.
- [52] A. Noshay, L.M. Robeson, Sulfonated polysulfone, *J. Appl. Polym. Sci.* 20 (1976) 1885–1903.
- [53] A. Dyck, D. Fritsch, S.P. Nunes, Proton-conductive membranes of sulfonated polyphenylsulfone, *J. Appl. Polym. Sci.* 86 (2002) 2820–2827.
- [54] Z. Jiang, X. Zhao, Y. Fu, A. Manthiram, Composite membranes based on sulfonated poly(ether ether ketone) and SDBS-adsorbed graphene oxide for direct methanol fuel cells, *J. Mater. Chem.* 22 (2012) 24862.
- [55] B.G. Choi, J. Hong, Y.C. Park, D.H. Jung, W.H. Hong, P.T. Hammond, H. Park, Innovative Polymer Nanocomposite Electrolytes: Nanoscale Manipulation of Ion Channels by Functionalized Graphenes, *ACS Nano.* 5 (2011) 5167–5174.
- [56] R.A. Mantz, P.F. Jones, K.P. Chaffee, J.D. Lichtenhan, J.W. Gilman, Thermolysis of Polyhedral Oligomeric Silsesquioxane (POSS) Macromers and POSS - Siloxane Copolymers, 4756 (1996) 1250–1259.
- [57] A. Fina, D. Tabuani, F. Carniato, A. Frache, E. Boccaleri, G. Camino, Polyhedral oligomeric silsesquioxanes (POSS) thermal degradation, *Thermochim. Acta.* 440 (2006) 36–42.
- [58] H. Fan, R. Yang, Thermal decomposition of polyhedral oligomeric octaphenyl, octa(nitrophenyl), and octa(aminophenyl) silsesquioxanes, *J. Therm. Anal. Calorim.* 116 (2014) 349–357.
- [59] H. Chabane, S. Livi, H. Benes, C. Ladavière, P. Ecorchard, J. Duchet-Rumeau, J. Gérard, Polyhedral oligomeric silsesquioxane-supported ionic liquid for designing nanostructured hybrid organic-inorganic networks, *Eur. Polym. J.* 114 (2019) 332–337.

- [60] M.J. Martínez-Morlanes, A.M. Martos, A. Várez, B. Levenfeld, Synthesis and characterization of novel hybrid polysulfone/silica membranes doped with phosphomolybdic acid for fuel cell applications, *J. Memb. Sci.* 492 (2015) 371–379.
- [61] L. Li, X. Li, R. Yang, Mechanical, thermal properties, and flame retardancy of PC/ultrafine octaphenyl-POSS composites, *J. Appl. Polym. Sci.* 124 (2012) 3807–3814.
- [62] M. Cypryk, Y. Apeloig, Mechanism of the Acid-Catalyzed Si–O Bond Cleavage in Siloxanes and Siloxanols. A Theoretical Study, *Organometallics*. 21 (2002) 2165–2175.
- [63] E.S. Park, H.W. Ro, C. V. Nguyen, R.L. Jaffe, D.Y. Yoon, Infrared Spectroscopy Study of Microstructures of Poly(silsesquioxane)s, *Chem. Mater.* 20 (2008) 1548–1554.
- [64] S. Mädler, K. Barylyuk, E. Boeri Erba, R.J. Nieckarz, R. Zenobi, Compelling Advantages of Negative Ion Mode Detection in High-Mass MALDI-MS for Homomeric Protein Complexes, *J. Am. Soc. Mass Spectrom.* 23 (2012) 213–224.
- [65] T. Nakai, Solid-state ^{29}Si NMR for Evaluating Microscopic Sites of Glass Materials: ^{29}Si Measurements in Multinuclear NMR, Most Efficient Measurements, Quantitative Measurements, *Advanced Measurements*, New Glas. 28 (2013) 17–28.
- [66] P.J. Launer, B. Arkles, Infrared analysis of organosilicon compounds: spectra-structure correlations, in: *Silicon Compd. Silanes Silicones*, Gelest Inc, Morrisville, PA, 2008: pp. 223–226.
- [67] C. del Río, E. Morales, P.G. Escibano, Nafion/sPOSS hybrid membranes for PEMFC. Single cell performance and electrochemical characterization at different humidity conditions, *Int. J. Hydrogen Energy*. 39 (2014) 5326–5337.
- [68] D. Joseph, N.N. Krishnan, D. Henkensmeier, J.H. Jang, S.H. Choi, H.-J. Kim, J. Han, S.W. Nam, Thermal crosslinking of PBI/sulfonated polysulfone based blend membranes, *J. Mater. Chem. A*. 5 (2017) 409–417.
- [69] W. Wu, Y. Li, J. Liu, J. Wang, Y. He, K. Davey, S. Qiao, Molecular-Level Hybridization of Nafion with Quantum Dots for Highly Enhanced Proton Conduction, *Adv. Mater.* 30 (2018) 1707516.
- [70] D. Gupta, A. Madhukar, V. Choudhary, Effect of functionality of polyhedral oligomeric silsesquioxane [POSS] on the properties of sulfonated poly(ether ether ketone) [SPEEK] based hybrid nanocomposite proton exchange membranes for fuel cell applications, *Int. J. Hydrogen Energy*. 38 (2013) 12817–12829.
- [71] K. Schmidt-Rohr, Q. Chen, Parallel cylindrical water nanochannels in Nafion fuel-cell membranes, *Nat. Mater.* 7 (2008) 75–83.
- [72] M.-M. Schiavone, D.H. Lamparelli, Y. Zhao, F. Zhu, Z. Revay, A. Radulescu, The Effects of Temperature and Humidity on the Microstructure of Sulfonated Syndiotactic–polystyrene Ionic Membranes, *Membranes*. 10 (2020) 187.
- [73] F. Beyraghi, S.H. Mirfarsi, S. Rowshanzamir, A. Karimi, M.J. Parnian, Optimal thermal treatment conditions for durability improvement of highly sulfonated poly(ether ether ketone)

- membrane for polymer electrolyte fuel cell applications, *Int. J. Hydrogen Energy*. 45 (2020) 13441–13458.
- [74] N. Lebert, N. Gay, E. Richaud, Mechanical and macromolecular changes during thermal degradation of polyphenylsulfone, *Polym. Degrad. Stab.* 195 (2022) 109812.
- [75] P. Zhang, W. Li, L. Wang, C. Gong, J. Ding, C. Huang, X. Zhang, S. Zhang, L. Wang, W. Bu, Polydopamine-modified sulfonated polyhedral oligomeric silsesquioxane: An appealing nanofiller to address the trade-off between conductivity and stabilities for proton exchange membrane, *J. Memb. Sci.* 596 (2020) 117734.
- [76] E. Lufrano, I. Nicotera, A. Enotiadis, M.H. Ur Rehman, C. Simari, Elucidating the Water and Methanol Dynamics in Sulfonated Polyether Ether Ketone Nanocomposite Membranes Bearing Layered Double Hydroxides, *Membranes*. 12 (2022) 419.
- [77] Z. Li, X. Hao, M. Xiao, S. Huang, D. Han, S. Wang, Y. Meng, Surface-Densified Non-Fluorinated Proton Exchange Membrane Used for Direct Methanol Fuel Cell, *J. Electrochem. Soc.* 170 (2023) 064502.
- [78] Z. Li, X. Hao, G. Cheng, S. Huang, D. Han, M. Xiao, S. Wang, Y. Meng, In situ implantation of cross-linked functional POSS blocks in Nafion® for high performance direct methanol fuel cells, *J. Memb. Sci.* 640 (2021).
- [79] Z. Wu, Y. Tang, D. Sun, S. Zhang, Y. Xu, H. Wei, C. Gong, Multi-sulfonated polyhedral oligosilsesquioxane (POSS) grafted poly(arylene ether sulfone)s for proton conductive membranes, *Polymer*. 123 (2017) 21–29.